Communication: Imaging wavefunctions in dissociative photoionization

W. Scott Hopkins and Stuart R. Mackenzie

Citation: The Journal of Chemical Physics **135**, 081104 (2011); doi: 10.1063/1.3632103
View online: http://dx.doi.org/10.1063/1.3632103
View Table of Contents: http://scitation.aip.org/content/aip/journal/jcp/135/8?ver=pdfcov
Published by the AIP Publishing

Communication: Imaging wavefunctions in dissociative photoionization

W. Scott Hopkins[a] and Stuart R. Mackenzie[b]
Department of Chemistry, University of Oxford, Physical and Theoretical Chemistry Laboratory, South Parks Road, Oxford OX1 3QZ, United Kingdom

(Received 20 July 2011; accepted 12 August 2011; published online 26 August 2011)

The dissociative ionization dynamics of excited electronic states of the xenon dimer, Xe_2, have been studied using velocity map ion imaging (VMI). A one-colour, (2+1) resonant excitation scheme was employed to first excite and then ionize selected vibrational levels of the Xe_2 $6p\ ^2[^1/_2]_0\ 0_g^+$ Rydberg state. Cationic fragments were then detected by the VMI. The data provide an outstanding example of the reflection principle in photodissociation with the full nodal structure of the Rydberg state wavefunctions clearly observed in the final Xe^+ kinetic energy distributions without the need for scanning the excitation energy. Fitting of the observed distributions provides detailed and precise information on the form of the Xe_2^+ $I(^1/_2g)$ potential energy curve involved which is in excellent agreement with the results of photoelectron imaging studies [Shubert and Pratt, J. Chem. Phys. **134**, 044315 (2011)]. Furthermore, the anisotropy of the product angular distributions yields information on the evolution of the electronic character of the ionic state with internuclear separation, R. The combination of the nature of dissociative ionization and the extent of the bound state wavefunctions provide information over an unusually wide range of internuclear separation R ($\Delta R > 0.75$ Å). This would normally require scanning over a considerable energy region but is obtained in these studies at a fixed excitation energy. © *2011 American Institute of Physics*. [doi:10.1063/1.3632103]

The velocity map imaging[1] (VMI) technique has become established as a powerful method for recording angular and quantum state distributions for the products arising from processes, such as photodissociation, photoionization/photodetachment, and reactive scattering.[2–4] These product state distributions (PSDs) intrinsically reflect the forces and torques acting between recoiling fragments during their evolution into isolated species and thus VMI studies provide important information on the nature of the potential energy surfaces involved in a fragmentation, ionization, or collision process.

Prompt dissociative photoionization, in which excitation occurs to a repulsive ionic potential energy curve (PEC), can be studied by both photoelectron and ion imaging variants of the VMI. In the case of a neutral diatomic molecule excited to a dissociative ionic state correlating with the ground state fragments, all excess energy is partitioned amongst the kinetic energies of the electron removed (eKE) and the cationic and neutral atom co-fragments (fragment kinetic energy release, fKER). The PSDs are governed by the Franck–Condon overlap of the neutral bound state wavefunctions and the continuum of ionic states. According to the reflection principle,[5–7] both the observed photofragment and photoelectron kinetic energy distributions should reflect the form of the probability density function (PDF) of the neutral level.[8] Here, we report a velocity map ion imaging study of the dissociative ionization of several vibrational levels of the Xe_2 $6p\ ^2[^1/_2]_0\ 0_g^+$ Rydberg state as illustrated schematically in Fig. 1.

The velocity map imaging time-of-flight (ToF) mass spectrometer employed has been described in detail previously but for these studies was operated without the laser ablation cluster source.[9,10] The xenon dimer, Xe_2, was produced by expanding a 20% mixture of Xe (BOC, 99.999%) in Ar (BOC, >99.9%) into the high vacuum source chamber via a pulsed solenoid valve (Parker Hannifin, series 9) from 8 bars stagnation pressure. The molecular beam was skimmed be-

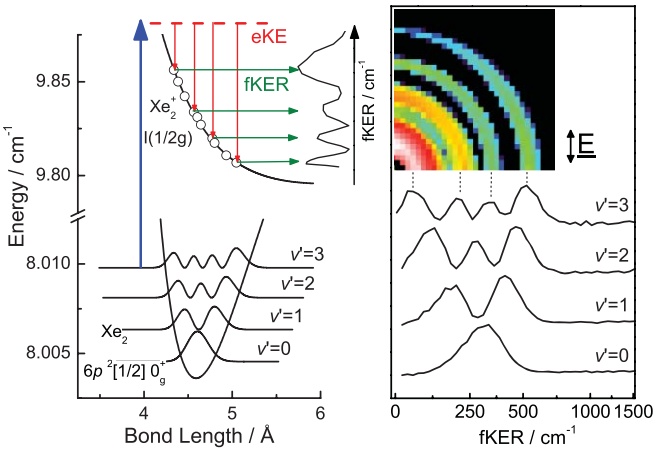

FIG. 1. (Left) Potential energy curves and bound state probability distribution functions involved in the dissociative ionization of Xe_2. The parameters for the $6p\ ^2[^1/_2]_0\ 0_g^+$ Rydberg state are taken from Refs. 12 and 13. Hollow circles indicate projection of the $6p\ ^2[^1/_2]_0\ 0_g^+(v')$ probability maxima on the Xe_2^+ $I(^1/_2g)$ state. (Right) The fKER spectra recorded following excitation from the Xe_2 $6p\ ^2[^1/_2]_0\ 0_g^+$ ($v' = 0$–3) levels and subsequent dissociative ionization. (Inset) A symmetrised quadrant of the reconstructed momentum space image recorded from the $0_g^+(v' = 3)$ level. E denotes the relative alignment of the photon electric vector.

[a]Present address: Department of Chemistry, University of Waterloo, Waterloo N2L 3G1, Canada.
[b]Author to whom correspondence should be addressed. Electronic mail: stuart.mackenzie@chem.ox.ac.uk.

fore being crossed by the tuneable, linearly polarized output of a frequency doubled pulsed dye laser at a repetition rate of 10 Hz (~500 μJ per 8 ns pulse, FWHM = 0.3 cm^{-1}). The ultraviolet beam was weakly focused with $f = 200$ mm MgF_2 spherical lens prior to entering the vacuum system, and the electric field vector of the laser was oriented so as to be parallel to the plane of the imaging detector. No attempt was made to clean up the polarization after the lens but we believe any polarization spoiling to be minimal as we have previously observed limiting values for anisotropy parameters with its use in this spectral region.[10,11]

The instrument operates in both linear time-of-flight and VMI modes. In linear ToF mode, the mass resolving power of the instrument is sufficient to observe the different isotopes (isotopologues) of Xe (Xe_2). Following photodissociation/ionization events of Xe_2 or Xe_2^+, expanding Newton spheres of Xe^+ fragments were extracted parallel with the molecular beam axis onto a commercial VMI detector (Photek). Mass selective detection was achieved by gating the detector assembly and the kinetic energy resolution in low kinetic energy release events was improved by the use of an extended drift tube of 759 mm. Images were recorded using a 586 × 776 pixel CCD camera and were analysed using a purpose built LABVIEW routine employing an onion peeling algorithm.[14]

The spectroscopy of the Rydberg states of Xe_2 has been explored in detail previously.[12,15–17] Electric dipole selection rules ($|\Delta\Omega| \leq 2, |\Delta J| \leq 2, g \leftrightarrow g$, and $+ \leftrightarrow +$) restrict two-photon excitation from the ground $X0_g^+$ state to 0_g^+, 1_g, or 2_g Rydberg states. The Xe_2 0_g^+ state, which correlates with the Xe* $5p^5 6p\ ^2[^1/_2]_0$ + Xe $5p^6\ (^1S_0)$ separated atom limit can be excited in the region of the strong atomic Xe $5p^5 6p\ ^2[^1/_2]_0 \leftarrow 5p^6\ (^1S_0)$ transition. Figure 2(a) shows

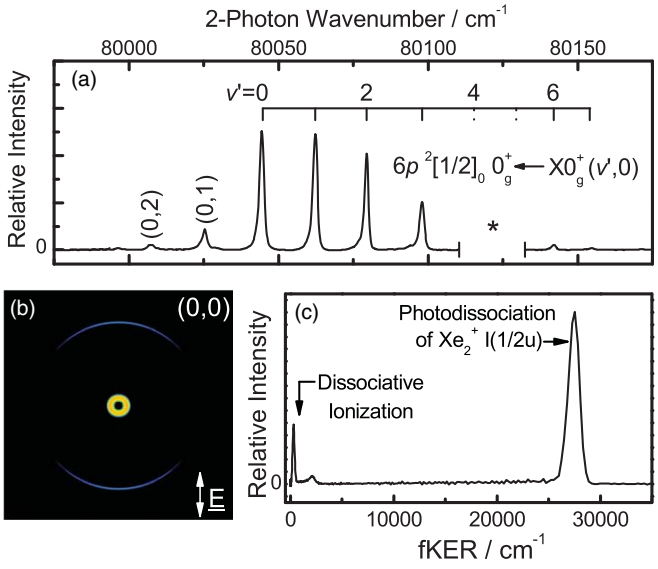

FIG. 2. (a) The Xe_2 $5p^5 6p\ ^2[^1/_2]_0\ 0_g^+ \leftarrow X0_g^+$ (2+1) REMPI spectrum in the 79 975–80 175 cm^{-1} region as observed in the Xe_2^+ mass channel. The asterisk, *, marks the Xe $5p^5 6p\ ^2[^1/_2]_0 \leftarrow 5p^6\ (^1S_0)$ atomic transition. (b) The reconstructed Xe^+ velocity map image observed following excitation of the Xe_2 $5p^5 6p\ ^2[^1/_2]_0\ 0_g^+ \leftarrow X0_g^+$ (0,0) transition at $2\nu \approx 80\,045$ cm^{-1}. (c) The fKER spectrum arising from the image in (b).

the Xe_2 $6p\ ^2[^1/_2]_0\ 0_g^+ \leftarrow X0_g^+$ spectrum as observed in the Xe_2^+ mass channel via (2+1) resonance enhanced multiphoton ionization (REMPI). An intense $v(', 0)$ progression is observed, with weaker features attributable to vibrational hot-bands from which a vibrational temperature of 15 ± 5 K is estimated.

The main features of the Xe_2 REMPI spectrum are reproduced in the Xe^+ mass channel indicating the presence of a competing dissociation channel. The Xe^+ VMI images recorded following excitation of the Xe_2 $6p\ ^2[^1/_2]_0\ 0_g^+ \leftarrow X0_g^+$ $(v', 0)$ transitions indicate Xe^+ production via two distinct mechanisms. One results in low fragment kinetic energy release of 0–750 cm^{-1} and another produces fragments with fKER ≈ 27 500 cm^{-1} as shown in the momentum space image reconstruction in Fig. 2(b) along with the corresponding fKER spectrum in Fig. 2(c). The total kinetic energy release may be calculated by summing fKER and the electron kinetic energy.

The low- and high-fKER product channels have been attributed previously to dissociative ionization of the Xe_2 Rydberg state and single-photon dissociation of Xe_2^+, respectively, and we confirm this interpretation.[18]

The high-fKER peaks can be assigned by energy balance calculations to single-photon dissociation of high-lying vibrational levels of the Xe_2^+ $I(^1/_2u)$ ground state, produced in the (2+1) REMPI process. The fKER spectra and angular distributions are consistent with single-photon excitation of the Xe_2^+ $I(^1/_2u)$ $v^+ \approx 60$ to the repulsive part of the Xe_2^+ $II(^1/_2g)$ state producing Xe $(^1S_0)$ + Xe^+ $(^2P_{1/2}{}^\circ)$ photofragments. This assignment agrees well with the recent Xe_2 photoelectron imaging study of Shubert and Pratt, in which Xe_2^+ $I(^1/_2u)$ $v^+ = 49$–87 production was observed and used in Franck–Condon simulations of the observed photoelectron bands to determine the bond length in the Xe_2 $6p\ ^2[^1/_2]_0\ 0_g^+$ intermediate state.[13]

The low-fKER dissociation channel products can be explained by projecting the Xe_2 $6p\ ^2[^1/_2]_0\ 0_g^+$ state PDFs, as determined using published molecular parameters,[12,13] onto the various low-lying electronic states of Xe_2^+.[19,20] The only ionic molecular state consistent with generation of low-fKER products is $I(^1/_2g)$, predicted to generate Xe^+ fKERs of <1500 cm^{-1} and correlated electron kinetic energies of ~22 000 cm^{-1} for the given (2+1) REMPI process. These eKEs accord well with the one-colour (2+1) photoelectron spectra of Shubert and Pratt,[13] in which a large peak spanning from EKE ≈ 21 000–25 000 cm^{-1} was observed, as well two-colour (2+1′) experiments, in which nodal PDF structure was identified and assigned as a minor photoionization contribution from the Xe_2^+ $I(^1/_2g)$ state.[13] The overall process is shown in Fig. 1.

Dissociation on the neutral potential energy surface followed by ionization of an excited atomic fragment may be discounted on energetic grounds: Only two dissociation channels are accessible at these energies and neither coincides with the fKER peaks observed.

Figure 3 shows the experimental Xe^+ VMI images recorded in the low-fKER region following excitation of the Xe_2 $6p\ ^2[^1/_2]_0\ 0_g^+ \leftarrow X0_g^+$ $(v' = 0–3, 0)$ transitions.

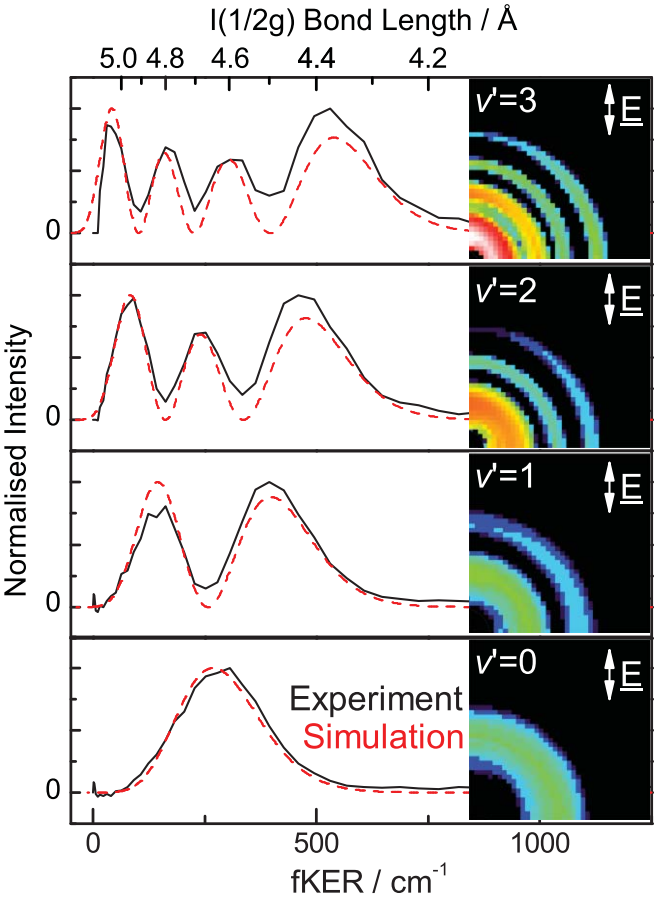

FIG. 3. Experimental (solid black) and simulated (dashed red) low-fKER distributions arising from dissociative ionization of the $6p\ ^2[^1/_2]_0\ 0_g^+$ (v' = 0–3) levels of Xe_2. The simulations use the reflection principle (Refs. 5 and 6) and assume a Morse potential form for the $Xe_2^+\ I(^1/_2g)$ state whose parameters have been fit to match the experimental data (see text).

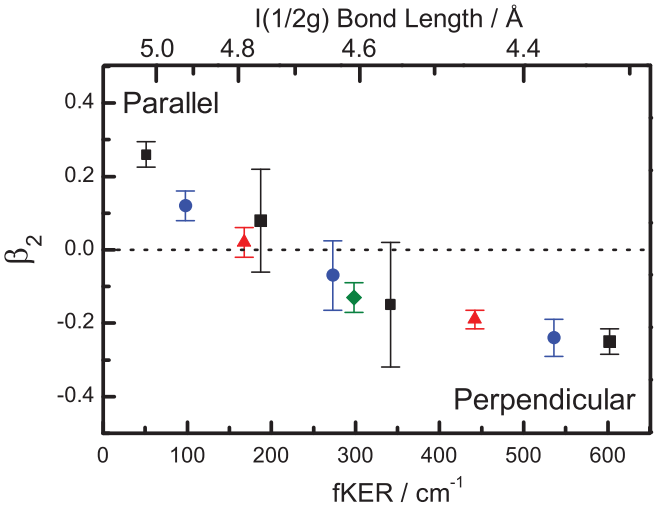

FIG. 4. Observed β_2 anisotropy parameters for the $Xe^+\ (^2P_{3/2}{}^\circ) + Xe\ (^1S_0)$ dissociative ionization channel as a function of fKER for excitation from the $Xe_2\ 6p\ ^2[^1/_2]_0\ 0_g^+$ $v' = 0$ (green diamond), $v' = 1$ (red triangles), $v' = 2$ (blue circles), and $v' = 3$ (black squares) levels. Points correspond to projection from local maxima in the vibrational level probability distributions. The indicated uncertainties represent one standard deviation. The upper scale represents the corresponding internuclear separation assuming the $Xe_2\ 6p\ ^2[^1/_2]_0\ 0_g^+$ parameters from Refs. 12 and 13.

They represent an unusually clear example of the reflection principle.[5,6] Due to the prompt ionization step, the $6p\ ^2[^1/_2]_0\ 0_g^+$ (v') PDFs are projected onto the repulsive wall of the $Xe_2^+\ I(^1/_2g)$ potential energy curve, upon which the molecular ion undergoes dissociation yielding Xe $(^1S_0)$ + Xe^+ $(^2P_{3/2}{}^\circ)$ products. The PDFs associated with the intermediate $6p\ ^2[^1/_2]_0\ 0_g^+$ (v') level wavefunctions are clearly manifested in the fKER spectra without the need for scanning the excitation laser.

In addition to the experimental distributions, Fig. 3 shows simulated fKER distributions. The simulations involved calculating wavefunction overlap integrals for the $Xe_2\ 6p\ ^2[^1/_2]_0\ 0_g^+$ $v' = 0$–3 vibrational levels and the $Xe_2^+\ I(^1/_2g)$ state continuum wavefunctions, followed by projecting the resulting PDFs into momentum space using the reflection principle. In fitting to the experimental data, the $Xe_2\ 6p\ ^2[^1/_2]_0\ 0_g^+$ was modeled by a Morse potential and the molecular parameters were fixed to those determined previously.[12,13] The ionic $Xe_2^+\ I(^1/_2g)$ state was assumed to be Morse-like, with the values for $D_e{}^+$ (72.9 cm^{-1}) and $R_e{}^+$ (6.096 Å) being fixed to those determined by Zehnder *et al.*,[20] and $\omega_e{}^+$ and $\omega_e x_e{}^+$ values optimized for agreement with experimental distributions. It is important to note, however, that only the repulsive wall of this potential is sampled in this study, not any bound region.

The calculated fKERs are exquisitely sensitive to the $Xe_2^+\ I(^1/_2g)$ state parameters and optimal values of $\omega_e{}^+ = 6.673 \pm 0.011\ cm^{-1}$ and $\omega_e x_e{}^+ = 0.1527 \pm 0.0005\ cm^{-1}$ could be extracted, with a fit R^2 value of 0.99817. These values are in excellent agreement with those determined by Shubert and Pratt.[13] It should be noted, however, that the fitted molecular parameters are highly correlated with the values for $D_e{}^+$ and $R_e{}^+$.

The VMI ion imaging data contain additional important information on the dissociative ionization process in the form of product angular distributions, which evolve from slightly parallel with the photolysis laser polarization to slightly perpendicular as a function of fKER. Figure 4 shows the β_2 anisotropy parameters extracted for dissociative ionization out of each vibrational level of the $Xe_2\ 6p\ ^2[^1/_2]_0\ 0_g^+$ Rydberg state. For completeness, the fits included higher order terms but the β_4 and β_6 parameters were found to be zero within experimental uncertainty. The data points in Fig. 4 correspond to observations made at each maximum in the corresponding PDF (the points representing the highest signal-to-noise ratio in the corresponding images). The wavefunction (and hence the PDF) for the $v' = 3$ level, extends across a wide range of internuclear separation $5.0 > R/Å > 4.3$ and we interpret the variation in product angular distributions as reflecting the gently changing electronic character of the dissociative $Xe_2^+\ I(^1/_2g)$ state as a function of bond length. This change is consequently reflected in the variation in the transition moment. A clear trend is observed from slightly parallel ($\beta_2 \approx +0.25$, corresponding to $\Delta\Omega = 0$ character) at low fKER to slightly perpendicular ($\beta_2 \approx -0.25$, $\Delta\Omega = \pm 1$) above fKER $= 200\ cm^{-1}$.

At relatively low fKER (i.e., the longest bond lengths probed), the $Xe_2^+\ I(^1/_2g)$ state is essentially unperturbed and contributes most strongly to the overall electronic character

of the ionic state. At shorter bond lengths (corresponding to higher fKER), the Xe_2^+ $I(^1/_2g)$ PEC crosses both the Xe_2^+ $I(^3/_2g)$ and $I(^3/_2u)$ potential energy curves.[20] The $I(^3/_2g)$ state, in particular, correlates with the same Xe $(^1S_0) + Xe^+$ $(^2P_{3/2}{}^\circ)$ separated atom limit as the $I(^1/_2g)$ state and can perturb it via a heterogeneous $\Delta\Omega = \pm 1$, $g \leftrightarrow g$ perturbation.[21] We propose that with decreasing internuclear separation there is an increasingly large $I(^3/_2g)$ contribution to the electronic state symmetry, resulting in the final excitation/ionization step evolving from a nominally perpendicular $0_g^+ \rightarrow I(^3/_2g) + e^-$ process at short internuclear distances to a nominally parallel $0_g^+ \rightarrow I(^1/_2g) + e^-$ process at longer internuclear distances.

An alternative interpretation of the observed trend in anisotropy lies in the R-dependence of the $I(^1/_2g)$ state character itself. With increasing internuclear separation, the system evolves from Hund's case (a), (b) angular momentum coupling to case (c). As a result, the $I(^1/_2g)$ state, a pure Π_g state in case (a) (corresponding to the $\sigma_g^2\pi_u^4\pi_g^3\sigma_u^2$ configuration), develops increasing Σ_g character in case (c) as a result of configuration mixing with the $\sigma_g^1\pi_u^4\pi_g^4\sigma_u^2$ configuration. The net effect of this mixing would be to increase the parallel nature of the electronic transition as observed.

The above interpretations of the anisotropy parameter both assume a fast dissociative photo-ionization process (at least compared with the rotational period), which is supported by the fact that non-zero β_2 values are extracted.

It is an unusual feature of the dissociative ionization process and the topology of the surfaces involved that information over a wide (>0.75 Å) range of internuclear separation can be obtained without the need for scanning the excitation energy. Indeed, most previous examples of the reflection principle, even those involving VMI, have involved scanning the full absorption spectrum in order to map the bound state wavefunction.[22] Whilst it is likely that this type of wavefunction measurement may be observed in other systems exhibiting prompt dissociative ionization, it is unlikely to be a general feature. In order to observe such a clear example as shown here, a fortuitous combination of curvature/slope for the bound and dissociative states is required. Too gentle a slope in the ionic state and the nodal structure will be highly compressed in the fKER spectrum, potentially beyond the resolution of the VMI technique. Too high a slope and the range of product kinetic energies will test the dynamic range of VMI. One highly appealing experiment would be a simultaneous photoelectron/photoion velocity map imaging experiment. Ultrafast variants of such photoelectron, photoion coincidence have already been applied to dissociative ionization of small polyatomic molecules.[23] In general, however, the possibility of rotational excitation of the fragments, as well as coupling of vibrational modes in larger systems may complicate the interpretation. Nevertheless, the mass of Xe and the correspondingly slow dynamics may permit some interesting picosecond experiments to be performed. Certainly, these results pose an intriguing possibility for an alternative means of determining the vibronic wavefunctions of molecules.

Funding for this research was provided by the Engineering and Physical Sciences Research Council (EPSRC, Grant No. EP/C012070). W.S.H. acknowledges funding from the Ramsay Memorial Fellowships Trust in the form of a Ramsay Memorial Fellowship. The authors gratefully acknowledge helpful discussions with Professor Mark S. Child during the data analysis and the assistance of Mr. Alex Woodham during acquisition of some of the data.

[1] A. Eppink and D. H. Parker, Rev. Sci. Instrum. **68**, 3477 (1997).
[2] M. N. R. Ashfold, N. H. Nahler, A. J. Orr-Ewing, O. P. J. Vieuxmaire, R. L. Toomes, T. N. Kitsopoulos, I. A. Garcia, D. A. Chestakov, S. M. Wu, and D. H. Parker, Phys. Chem. Chem. Phys. **8**, 26 (2006).
[3] A. Sanov and R. Mabbs, Int. Rev. Phys. Chem. **27**, 53 (2008).
[4] A. I. Chichinin, K. H. Gericke, S. Kauczok, and C. Maul, Int. Rev. Phys. Chem. **28**, 607 (2009).
[5] M. Shapiro, Chem. Phys. Lett. **81**, 521 (1981).
[6] M. S. Child and M. Shapiro, Mol. Phys. **48**, 111 (1983).
[7] M. S. Child, H. Essen, and R. J. Leroy, J. Chem. Phys. **78**, 6732 (1983).
[8] R. Schinke, *Photodissociation Dynamics: Spectroscopy and Fragmentation of Small Polyatomic Molecules* (Cambridge University Press, Cambridge, England, 1993).
[9] W. S. Hopkins, S. M. Hamilton, P. D. McNaughter, and S. R. Mackenzie, Chem. Phys. Lett. **483**, 10 (2009).
[10] W. S. Hopkins, A. P. Woodham, R. J. Plowright, T. G. Wright, and S. R. Mackenzie, J. Chem. Phys. **134**, 094311 (2011).
[11] W. S. Hopkins, A. P. Woodham, R. J. Plowright, T. G. Wright, and S. R. Mackenzie, J. Chem. Phys. **132**, 214303 (2010).
[12] S. S. Dimov, J. Y. Cai, and R. H. Lipson, J. Chem. Phys. **101**, 10313 (1994).
[13] V. A. Shubert and S. T. Pratt, J. Chem. Phys. **134**, 044315 (2011).
[14] G. M. Roberts, J. L. Nixon, J. Lecointre, E. Wrede, and J. R. R. Verlet, Rev. Sci. Instrum. **80**, 053104 (2009).
[15] P. M. Dehmer, S. T. Pratt, and J. L. Dehmer, J. Chem. Phys. **85**, 13 (1986).
[16] S. S. Dimov, X. K. Hu, D. M. Mao, and R. H. Lipson, Chem. Phys. Lett. **239**, 332 (1995).
[17] X. K. Hu, D. M. Mao, S. S. Dimov, and R. H. Lipson, Phys. Rev. A **54**, 2814 (1996).
[18] V. A. Shubert, M. Rednic, and S. T. Pratt, J. Chem. Phys. **132**, 124108 (2010).
[19] K. Vasilatou, U. Hollenstein, and F. Merkt, Mol. Phys. **108**, 915 (2010).
[20] O. Zehnder, R. Mastalerz, M. Reiher, F. Merkt, and R. A. Dressler, J. Chem. Phys. **128**, 234306 (2008).
[21] G. Herzberg, *Molecular Spectra and Molecular Structure I. Spectra of Diatomic Molecules*, 2nd ed. (Van Nostrand Reinhold, Toronto, 1939).
[22] E. Wrede, S. Laubach, S. Schulenburg, A. Brown, E. R. Wouters, A. J. Orr-Ewing, and M. N. R. Ashfold, J. Chem. Phys. **114**, 2629 (2001).
[23] J. A. Davies, J. E. LeClaire, R. E. Continetti, and C. C. Hayden, J. Chem. Phys. **111**, 1 (1999).